Bulletin of the Seismological Society of America, Vol. 77, No. 2, pp. 420–439, April 1987

THE EFFECT OF CRUSTAL STRUCTURE ON STRONG GROUND MOTION ATTENUATION RELATIONS IN EASTERN NORTH AMERICA

BY R. W. BURGER, P. G. SOMERVILLE, J. S. BARKER, R. B. HERRMANN, AND D. V. HELMBERGER

ABSTRACT

Strong ground motion attenuation relations are usually described by smoothly decreasing functions of distance. However, consideration of wave propagation in the crust suggests that attenuation relations should be more complex. Such complexity may be present in strong ground motion data for eastern North American earthquakes, which show amplitudes in the distance range of 60 to 150 km that lie above the trends at smaller and greater distances. Using a wavenumber integration method to compute Green's functions and close-in recordings of several earthquakes as empirical source functions, we have generated synthetic seismograms that are in good agreement with regional and strong-motion recordings of eastern North American earthquakes. From these synthetic seismograms, we have shown that the observed interval of relatively high amplitudes may be attributable to postcritically reflected *S* waves from the Moho. The presence and location of the interval of relatively high amplitudes is highly dependent on the crustal velocity structure and may therefore be expected to show regional variation. However, for any realistic structure model, there will be a transition in the attenuation relation from an interval at shorter distances (less than about 100 km) that is dominated by direct waves to an interval at greater distances that is dominated by postcritically reflected waves. The synthetic seismograms have response spectral velocities that match those of the recorded data, and their m_{bLg} values are in good agreement with observed values.

INTRODUCTION

The strong ground motion data that are available to constrain attenuation relations in eastern North America (e.g., Eckert and Atkinson, 1985) are quite sparse, but suggest high amplitudes in the distance range of 60 to 150 km, compared with the trends at smaller and greater distances. It is important to evaluate whether this feature reflects average ground motion characteristics or is due to anomalous data. In the absence of a larger data set with which to assess this question, it is appropriate to use synthetic seismograms to simulate strong ground motion characteristics. This approach is becoming increasingly important in the evaluation of ground motions for seismic design, especially in regions such as eastern North America where earthquakes are relatively infrequent and strong ground motions are correspondingly sparse.

A variety of methods for the simulation of strong ground motion characteristics is now available. One common approach uses random vibration theory (Hanks and McGuire, 1981; Boore, 1983) in which amplitude decay and wave-packet duration are prescribed functions of distance. Attenuation relations derived using this method have amplitudes which smoothly decay with distance. In this respect, they are similar to attenuation relations derived from empirical data, in which the decay with distance is fit using a smoothly decreasing functional form.

Consideration of wave propagation through a layered structure suggests that the dependence of ground motion amplitude on distance may have a more complex form due to the dominance of individual seismic phases over specific distance

ranges. One such phase that is known to be potentially large within the distance range of interest is the S-wave postcritically reflected at the Moho (e.g., Helmberger and Malone, 1975). It is of interest to determine whether phases such as this can explain the relatively large ground motions that are observed in the distance range of 60 to 150 km.

Recent theoretical studies on the propagation of regional seismic waves through a crustal structure have used synthetic seismogram methods (e.g., Bouchon, 1982; Langston, 1982). Following these and other such studies, we have adopted a synthetic seismogram approach which explicitly includes the effect of structure. Complete Green's functions for a simple crustal structure were computed using a frequency-wavenumber integration approach (Barker, 1984). The crustal structure used in our simulations was selected to represent the crust in maritime Canada.

To provide comparisons of the synthetic seismograms with observed data, seismograms from specific earthquakes recorded by the Eastern Canada Telemetered Network (ECTN) were chosen for comparison with the synthetic ground motions. To investigate ground motion attenuation with distance, the 1982 New Hampshire event was chosen because it generated strong motion recordings over a wide range of epicentral distances. To include the effects of source function complexity and receiver interactions in our deterministic models, we have used a strong motion recording at a distance of 8 km from the New Hampshire event as an empirical source function.

In order to further validate our ground motion simulations, we have compared the character of the synthetic and observed L_g waves, and compared synthetic and observed m_{bLg} values. Using strong motion recordings of a series of earthquakes, we have examined the relationship between seismic moment and m_{bLg} using synthetic seismograms, and compared the results with empirical data.

Simulated Strong-Motion Seismograms

Figure 1 shows a profile of synthetic vertical displacement seismograms for a vertical strike-slip dislocation along a 45° azimuth. The crustal structure model used to compute the Green's functions is given in Table 1 and was selected to represent the crust in maritime Canada. The synthetic seismograms were computed for a source depth of 7 km and include all the crustal arrivals. Green's functions have been convolved with a Brune (1970) source function with a 4.0 Hz corner frequency. The synthetic seismogram at 135 km shows some of the more important seismic arrivals. In particular, at this distance the S waves reflected off the Moho (SmS) are particularly large. This effect has been documented in other studies (e.g., Helmberger and Malone, 1975). The peak ground displacement remains constant and even increases slightly over the range of 60 to 135 km.

The synthetic seismograms shown in Figure 1 are much simpler than typical recorded seismograms. This may be due, in part, to the fact that our synthetic seismograms have not included the effects of scattering. However, the mismatch may also be partly due to the rather simple source-time history and receiver functions used. In an attempt to incorporate the high-frequency complexities of the source function and receiver interactions, we used a tangential component accelerogram recorded at 8 km from the 1982 Gaza, New Hampshire, earthquake as an empirical source function. This method of combining an empirical source function with computed Green's functions to simulate ground motions has been described by Hadley *et al.* (1982). Figure 2 shows the observed New Hampshire accelerogram used, and its corresponding displacement time series and amplitude spectrum. The

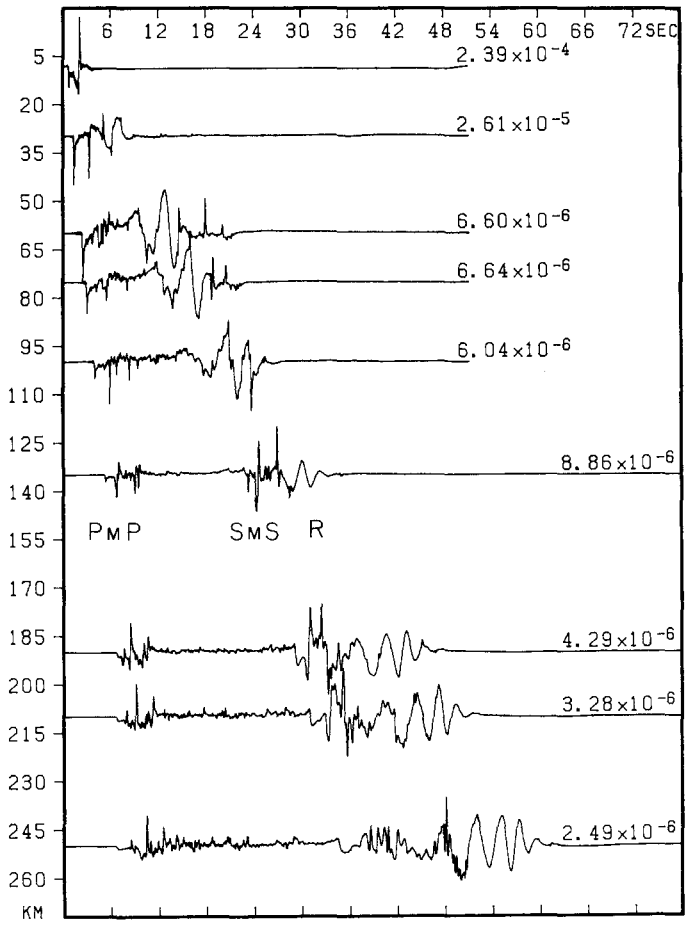

FIG. 1. Profile of synthetic vertical displacement seismograms for a vertical strike-slip mechanism seen at 45° azimuth. The source function is a Brune source with a 4.0 Hz corner frequency. Peak amplitudes are given in centimeters for a moment of 10^{20} dyne-cm.

TABLE 1

MARITIME CANADA CRUSTAL MODEL

P Velocity (km/sec)	*S* Velocity (km/sec)	Density (gm/cm^3)	Thickness (km)	*Q*-alpha	*Q*-beta
5.4	3.1	2.4	0.5	500	250
5.8	3.3	2.5	3.0	1000	500
6.35	3.7	2.8	26.5	1000	500
7.35	4.0	2.92	10.0	1000	500
8.33	4.75	3.39	—	1000	500

displacement record will serve as the empirical source function used to compute synthetic seismograms for a typical event of this magnitude (and corresponding moment and source duration). Later in the paper, we will compute synthetic seismograms for events with larger moments by using close-in recordings from different events having the desired seismic moments. Table 2 gives previously determined source parameters for these events.

Figure 3 shows a profile of vertical displacement seismograms obtained by convolving Green's functions with the empirical source function. The New Hamp-

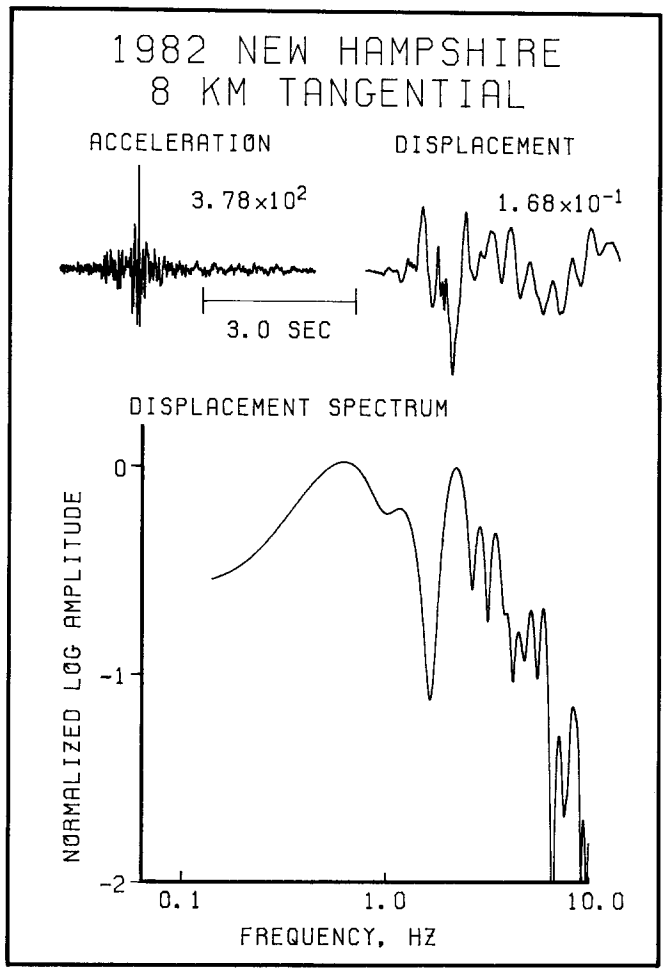

FIG. 2. Observed tangential component acceleration record, and the corresponding displacement time series and amplitude spectrum from the 1982 New Hampshire earthquake at a distance of 8 km (Franklin Falls downstream). Amplitudes are in c.g.s. units. The displacement spectrum has been normalized to a Brune source spectral shape.

TABLE 2

PARAMETERS OF EMPIRICAL SOURCE FUNCTIONS

	New Hampshire	Coyote Lake	San Fernando
Seismic moment (dyne-cm)	6.0×10^{22}	3.0×10^{24}	8.0×10^{25}
Source duration (sec)	0.4	2.0	6.0
Strong-motion station	Franklin Falls downstream	Coyote Creek	Pacoima Dam
Component*	Tangential	Radial	Radial
Closest distance to fault	8 km	1 km	3 km
Reference	Sauber (1984)	Liu and Helmberger (1983)	Langston (1978)

*Approximate orientation with respect to epicenter.

shire event has a corner frequency (about 2.5 to 5.0 Hz) similar to that of the Brune source in Figure 1. The empirical source spectrum shown in Figure 2 has been scaled to have the same long-period level and overall spectral shape as a Brune source. Thus, the profiles shown in Figures 1 and 3 differ only in the complexity of

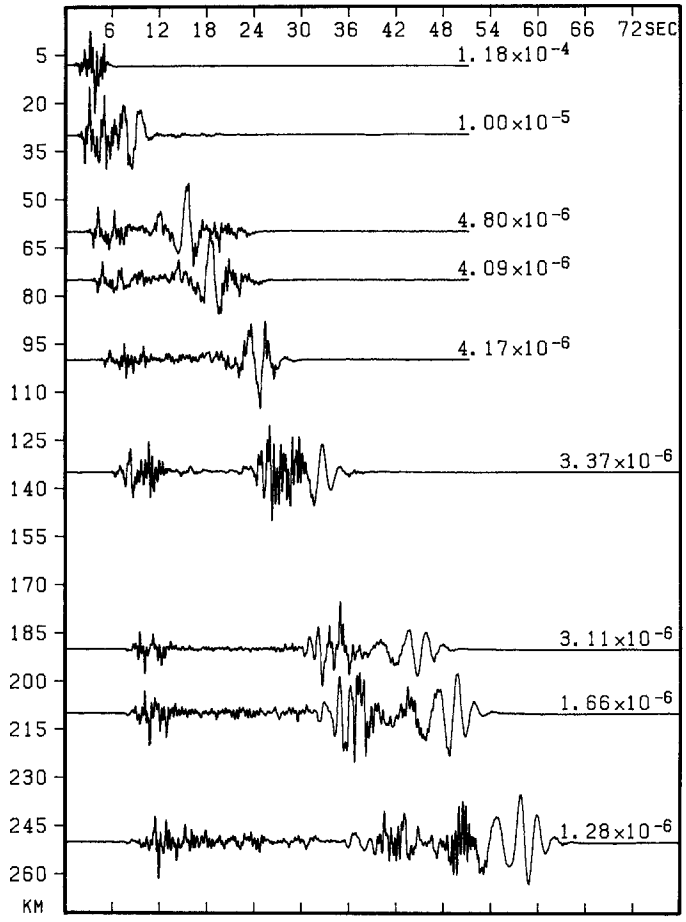

FIG. 3. Profile of synthetic vertical displacement seismograms for a vertical strike-slip mechanism seen at 45° azimuth. The source function is the observed displacement record in Figure 2. Peak amplitudes are given in centimeters for a moment of 10^{20} dyne-cm.

the source function and not the overall frequency content. The implicit assumption that the 8 km record represents only the source function is obviously oversimplified, since the 8 km record contains some effects due to structure. However, the added complexities introduced by using it as the source-time function can be considered to approximate near-receiver scattering phenomena. The presence of propagation effects as well as the high-frequency source components in the observed accelerogram result in synthetic seismograms (Figure 3) that appear to be considerably more realistic than those shown in Figure 1.

Figure 4 shows the observed vertical velocity seismograms for the New Hampshire event at the ECTN stations SBQ and MNT, along with the synthetic velocity seismograms. The New Hampshire focal mechanism is approximately: strike-N20°E; dip = 80°; and rake = −160° (Sauber, 1984). The source depth is about 3 to 4 km (Sauber, 1984) and is not very different from the source depth used in our simulations (7 km). The S minus P arrival times, peak amplitudes, and the general character of the observed waveforms in Figure 4 are fairly well-matched by the synthetic seismograms. [The synthetic for MNT was computed for a different distance (250 km) than the observed (274 km) seismogram, probably adding to the mismatch at that station.] However, the observed P waves are not as large as the

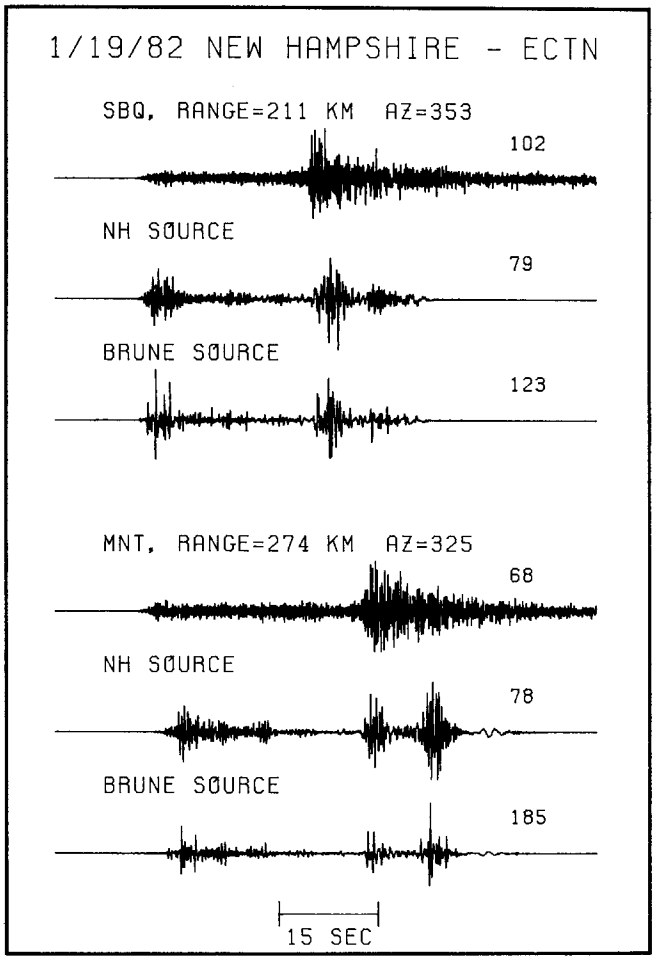

FIG. 4. Vertical velocity seismograms of the 1982 New Hampshire earthquake recorded at ECTN stations SBQ and MNT compared with the synthetic seismograms using the empirical source function and the Brune source function. Peak amplitudes are given in 10^{-4} cm/sec.

synthetic ones. Also, the two S-wave trains in the synthetic seismograms are not as clear in the observed seismograms. These differences are attributed to inadequacies in our crustal model. For example, a crustal model with a different velocity gradient will turn the rays at different angles of incidence, affecting the P-to-S amplitude ratio. Also, the observed seismograms have longer coda than the synthetic seismograms, which indicates that scattering is present in the observed seismograms but was not fully accounted for in the generation of synthetic seismograms. This may explain why the two S-wave trains are not as distinct in the data. The synthetic seismograms generated using the Brune source function appear to be too simple to explain the observed seismograms, even allowing for inadequacies in the synthetic seismograms related to crustal structure and scattering.

To extend the comparison of recorded and synthetic seismograms, we examined several of the Miramichi, New Brunswick, earthquakes. Observed and synthetic vertical velocity seismograms for ECTN recordings of the 31 March 1982 New Brunswick aftershock are shown in Figure 5. The New Hampshire record at 8 km is used as the source function for this event, since the magnitudes of the two events

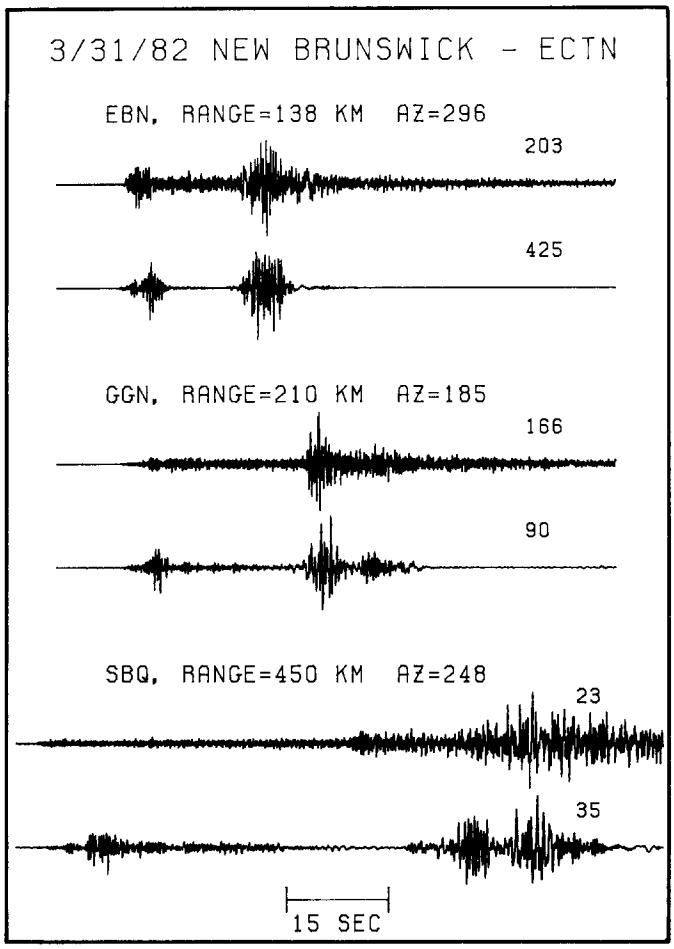

FIG. 5. Vertical velocity seismograms of the 31 March 1982 New Brunswick aftershock recorded at ECTN stations EBN, GGN, and SBQ (*upper traces*) compared with synthetic seismograms at comparable distances and azimuths using the empirical source function (*lower traces*). Peak amplitudes are given in 10^{-4} cm/sec.

are similar. The agreement between the synthetic and observed seismograms is good, and is generally better than that for the observed New Hampshire seismograms shown in Figure 4. This suggests that the crustal model used in generating the synthetic seismograms, which was selected for maritime Canada, is in fact more appropriate there than in New England.

The comparisons of observed and synthetic seismograms shown in Figures 4 and 5 provide a validation of our method of computing synthetic seismograms. Further validation of our method comes from the matching of L_g amplitudes from the ECTN data (Figures 4 and 5), and of WWSSN L_g magnitudes over a wide range of seismic moments, as described later in the paper. However, the comparison of observed and synthetic waveforms also indicates the need to use more realistic crustal structure models and to incorporate the effects of scattering in order to more closely match the observed seismograms. Nevertheless, our simplified structure model provides a useful means of examining the effect of structure on strong ground motion attenuation.

Ground Motion Attenuation Relations

The dependence of horizontal pseudo-velocity at 1 Hz and 5 per cent damping on epicentral distance obtained from strong-motion recordings of earthquakes in eastern North America (Eckert and Atkinson, 1985) is shown in Figure 6. Pseudo-velocity is the peak in the response of passing an accelerogram through a harmonic oscillator with a given natural frequency and a given damping factor. The pseudo-velocities in Figure 6 have been corrected so that the m_{bLg} for each earthquake is normalized to 5. Although the data are sparse for distances less than 100 km, it appears that certain distinct trends can be recognized. The amplitudes decrease over the distance range 10 to 60 km, but at about 60 km there is a discontinuity in slope, with amplitudes remaining constant out to about 150 km. At about 150 km, there is a discontinuity in amplitude level, with amplitudes dropping abruptly and then proceeding to decay more gradually. This interpretation of the observed data is shown as the solid curve in Figure 6. The 1 Hz pseudo-velocities for the New Hampshire event alone (letter F), which are shown as circles in Figure 7, are not inconsistent with these trends. The data denoted by the lowercase b in Figure 6 (from a New Madrid earthquake) at distances around 100 km may be significantly affected by site effects. However, our interpretation of the data is based primarily on the New Hampshire event data, and other earthquake data not affected by site efects (uppercase letters).

To simulate the attenuation relation shown in Figure 6, we computed a synthetic accelerogram profile for the New Hampshire event. Pseudo-velocities at 1 Hz were computed from the tangential component synthetic accelerograms at an azimuth of 210°. The resulting dependence of pseudo-velocity on distance is shown in Figure 7

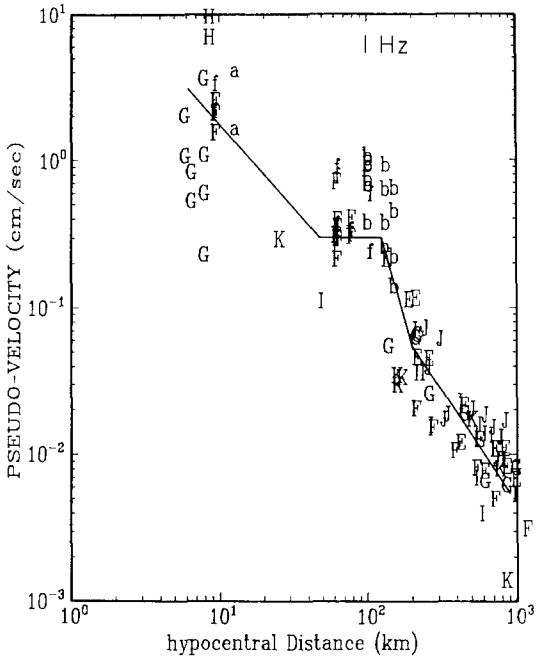

FIG. 6. Observed pseudo-velocities at 1 Hz and 5 per cent damping, normalized to $m_{bLg} = 5$, shown as a function of hypocentral distance for eastern North America earthquakes (modified from Eckert and Atkinson, 1985). The different letters represent data from different earthquakes, and lowercase letters represent recordings that may be significantly affected by site effects. The lines represent an interpretation of the data that is described in the text.

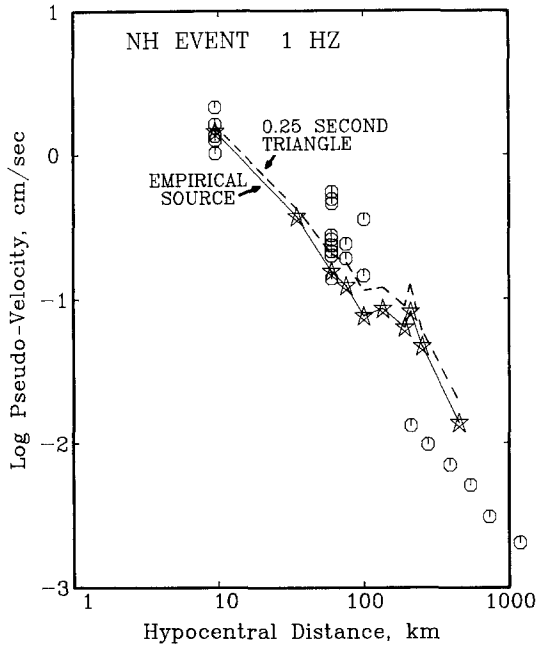

FIG. 7. Synthetic tangential pseudo-velocities at 1 Hz and 5 per cent damping (stars) as a function of hypocentral distance for the 1982 New Hampshire event using the empirical source function. The observed mean horizontal values are shown as circles. The dashed line represents the synthetic attenuation relation using a 0.25 sec (4 Hz) triangle source function.

together with the observed data. The observed and synthetic pseudo-velocities are absolute values for the observed L_g magnitude and the source parameters listed in Table 2. Thus, the synthetic values can be compared directly with the data.

The synthetic attenuation relation shown in Figure 7 shows three trends that are similar to those in the observed data. The logarithms of the pseudo-velocities decay with distance with a slope of about 1.2 out to 100 km, with amplitudes then remaining constant out to 200 km before abruptly decreasing again. The amplitudes of the synthetic seismograms are in good agreement with the observed values at distances out to 80 km. We will show in the next section that the interval of constant pseudo-velocity amplitudes between 100 and 200 km is due to large-amplitude postcritically reflected S waves from the Moho and from the interface at 30 km depth (hereafter referred to as "Moho reflections").

Synthetic accelerograms using a triangular source function having a corner frequency of 4 Hz were generated and used to examine the effect on the attenuation relation of neglecting complexities in the source and receiver functions. The triangular source attenuation relation, shown in Figure 7 as the dashed line, is quite similar to that obtained using the empirical source function, indicating that structure is the key factor in determining the form of the distance decay. The pseudo-velocities are smaller for the empirical source than for the triangular source because the use of the empirical source tends to smear out the more impulsive spikes compared to the triangular source, thereby reducing the peak response.

To interpret the synthetic attenuation relations, we performed generalized ray calculations (Helmberger and Harkrider, 1978) for a subset of arrivals using the maritime Canada structure model. The rays used in these calculations are shown in Figure 8 and represent some of the more important primary arrivals in the complete

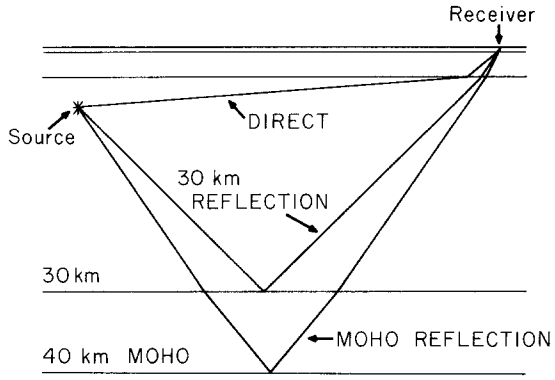

FIG. 8. Paths of the direct ray and rays reflected off the 30 km interface and the Moho (at 40 km depth).

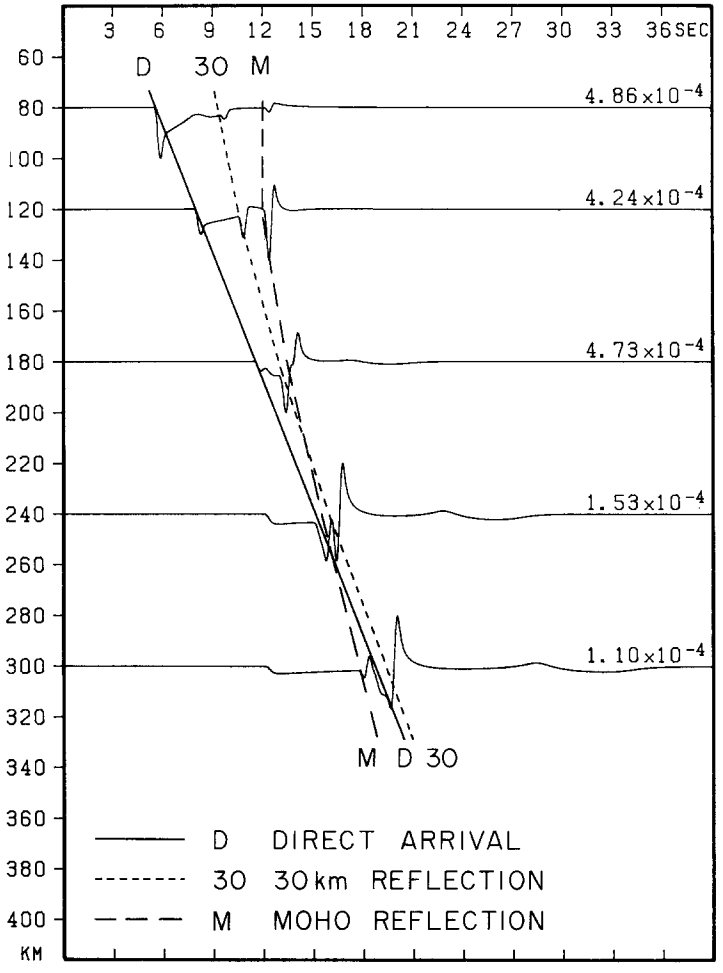

FIG. 9. Synthetic tangential displacement seismograms calculated from the three rays shown in Figure 8. The mechanism is a vertical strike-slip source seen at 0° azimuth. A trapezoidal time function (0.2, 0.1, 0.2) was used as the source function.

calculations. Figure 9 shows the large variation with range in the synthetic tangential displacement seismograms for the rays shown in Figure 8. At the closest ranges, the direct arrival dominates the waveform; but at larger ranges, reflections from discontinuities at depth begin to become more important. This is because these rays become postcritically reflected off these boundaries, such that all of the energy is reflected upward, and none is transmitted into the mantle.

Figure 10 shows the amplitudes of the individual arrivals (solid lines) and ray sum (dashed line) as a function of distance. The range at which the Moho reflection becomes postcritical is about 120 km and is indicated by the abrupt increase in amplitude of that ray. Beyond that range, that individual arrival follows an amplitude decay with distance similar to that of the direct ray, but with a larger amplitude. The same feature is shown with the reflection from the layer interface at a depth of 30 km as it becomes postcritical at about 180 km. The effect of these arrivals on the amplitude decay of the ray sum seismograms is to create a shoulder or bump in the attenuation relation. This region of fairly constant amplitudes simulated with

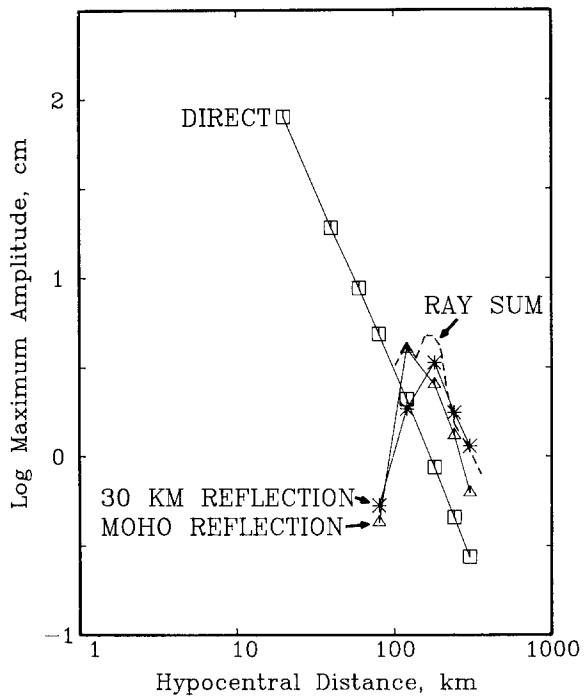

FIG. 10. Peak ground displacement as a function of hypocentral distance for the three individual rays (solid) and the ray sum (dashed) from the synthetic seismograms shown in Figure 9.

TABLE 3

CENTRAL UNITED STATES CRUSTAL MODEL

P Velocity (km/sec)	*S* Velocity (km/sec)	Density (gm/cm^3)	Thickness (km)	*Q*-alpha	*Q*-beta
5.0	2.89	2.5	1.0	100	50
6.1	3.52	2.7	9.0	1515	757
6.4	3.7	2.9	10.0	8000	4000
6.7	3.87	3.0	20.0	8000	4000
8.15	4.7	3.4	—	8000	4000

the reduced number of arrivals is similar to the one simulated with the complete seismograms shown in Figure 7.

The interval of constant ground motion amplitudes (between 60 and 150 km) from our interpretation of the observed data can be attributed to postcritical Moho reflections. In the synthetic seismograms, the Moho reflections cause constant amplitudes over the distance range of 100 to 200 km. This range is dependent on the focal depth, crustal thickness, and the crustal velocity gradient. To illustrate the effect of a different structure model, we present the ground motion attenuation for a crustal structure appropriate for the Central United States (given in Table 3; from Herrmann, 1985). Complete synthetic velocity seismograms were computed for a 5-km-deep source, with a 0.5 sec symmetric source function, and a moment of 10^{20} dyne-cm. The synthetic seismograms were passed through a 1.25 Hz high-pass filter (to emulate ECTN instruments). To estimate the variation induced by focal mechanism differences, synthetic seismograms were computed for 10° increments of dip and strike and 20° increments of slip, and then the peak velocities were averaged over all orientations.

Figure 11 presents the average with standard deviation of the peak tangential velocity as a function of hypocentral distance. The attenuation relation shown in Figure 11 behaves much as the synthetic attenuation relation given in Figure 7, except that the range of high amplitudes is between 60 and 150 km for the Central United States crustal model rather than between 100 and 200 km for the maritime Canada crustal model. The crustal thickness is the same for both models, but the velocity contrast at the Moho is larger for the Central United States model. Thus, the angle (and consequently range) at which the reflection off the Moho becomes

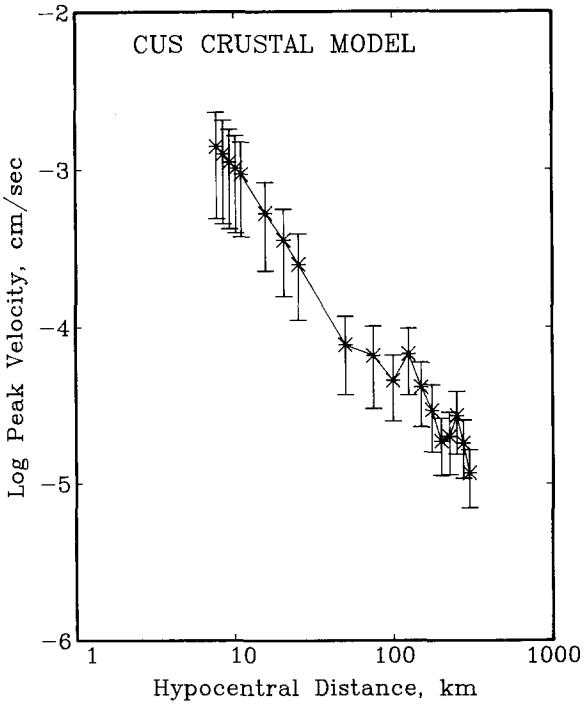

FIG. 11. Average peak tangential velocity as a function of hypocentral distance for the Central United States crustal model. The averages and standard deviations from calculations for 4536 focal mechanisms are shown. Similar effects are seen on the vertical, radial, and total horizontal components.

postcritical is different. The effect is to cause the region of high amplitudes to be at shorter distances for the Central United States model compared to the maritime Canada model. The range of observed high amplitudes in eastern North America (Figure 6) appears to be better matched by the Central United States crustal model than by our maritime Canada crustal model.

L_g Waves and the Relation between L_g Magnitude and Seismic Moment

Since L_g waves control strong ground motion amplitudes at the greater distances, a successful method of simulating strong motions should also be able to simulate recorded L_g waves and the empirical relation between m_{bLg} and seismic moment. The relation between L_g magnitude and seismic moment is well defined by the empirical data shown as circles in Figure 12, which also includes synthetic results described below. The seismic moments, which are based on waveform modeling methods, are described by Somerville *et al.* (1987, this volume), and the L_g magnitudes are from the Electric Power Research Institute (1985) earthquake catalog.

Accordingly, to further validate our synthetic seismogram computations, we calculated m_{bLg} from synthetic seismograms for a range of seismic moment values and compared them with observed moment-magnitude values. Short-period WWSSN synthetic L_g seismograms for the empirical New Hampshire source function and a 4.0 Hz Brune source are shown in Figure 13 for a range of 250 km. The synthetic seismograms are for the New Hampshire source mechanism as observed at an azimuth of 350°. The magnitudes given are for the L_g phase (group velocity 3.3 to 3.5 km/sec) and are calculated by the relation given by Herrmann and Kijko (1983b). The observed WWSSN value for this event is 4.6, and the observed ECTN value is 4.8. The magnitudes obtained from the synthetic seismograms using the empirical source and the Brune source are 5.00 and 5.25, respectively. The magnitude from the empirical source synthetic seismogram is in moderate agreement with the

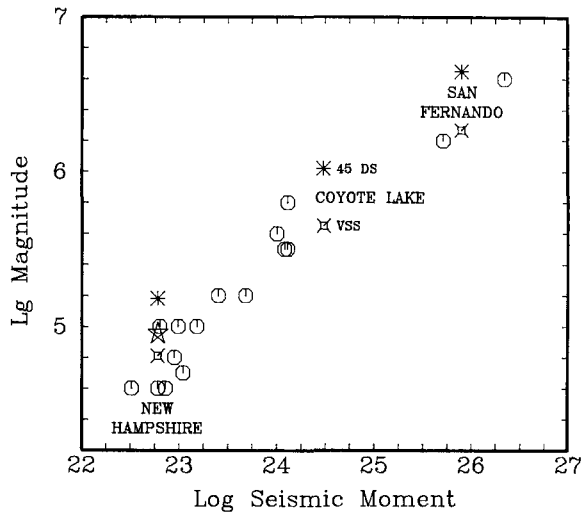

FIG. 12. L_g magnitude as a function of seismic moment for eastern North American earthquakes. The circles are observed data. The other symbols represent azimuthally averaged magnitudes obtained from synthetic seismograms for a range of 250 km using local recordings of the New Hampshire, Coyote Lake, or San Fernando earthquakes as empirical source functions. Asterisks and squares correspond to 45° dip-slip and vertical strike-slip mechanisms, respectively. The star represents the mechanism of the New Hampshire earthquake.

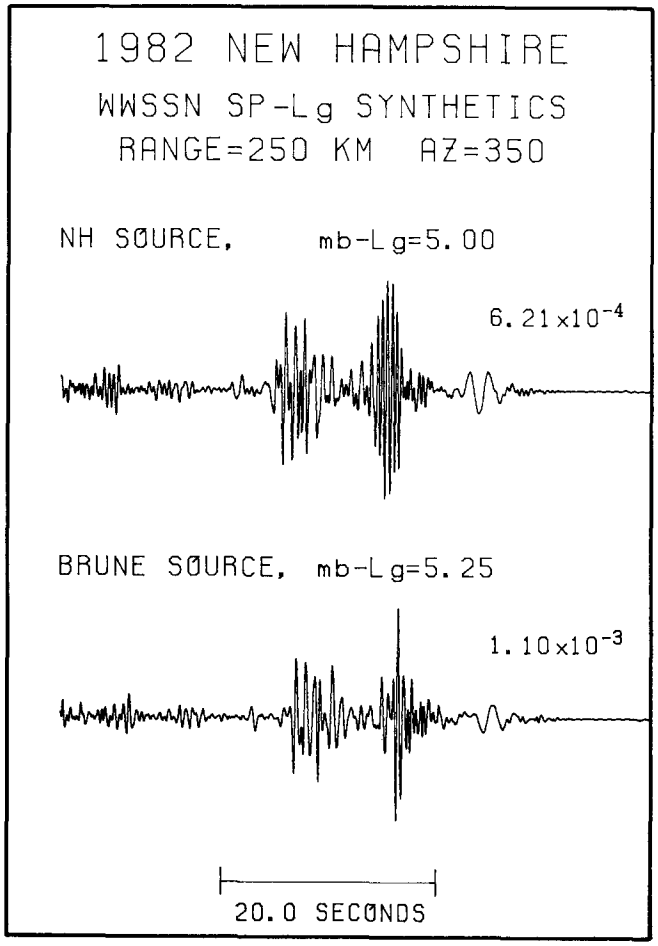

FIG. 13. Synthetic L_g waves and magnitudes for the 1982 New Hampshire event using both the empirical source function and the Brune source function. The synthetic seismograms are for a distance of 250 km seen at 45° azimuth. Peak amplitudes are given in centimeters.

observed magnitude. The L_g magnitudes from the synthetic seismograms at 450 km are 5.00 and 5.14, respectively. The L_g magnitude obtained by averaging the values from synthetic seismograms with the empirical New Hampshire source over 15° increments of azimuth at 250 km is 4.96 and is shown as the star in Figure 12. The use of the empirical source function tends to smear out the more impulsive spikes compared to the Brune source synthetic seismogram, thereby reducing the maximum amplitude to a more realistic level and lengthening the coda duration. Further reduction to a level more consistent with the data could be obtained by including scattering effects in the synthetic seismograms.

To determine a synthetic L_g magnitude-seismic moment relation, synthetic seismograms were computed using three empirical source functions with different seismic moments (and corresponding different source durations). In the absence of strong motion recordings from larger eastern North American earthquakes that could be used as empirical source functions, we have used recordings from California earthquakes. The close-in strong motion recordings that are used as empirical sources (in addition to the 1982 New Hampshire earthquake) are from the 1979 Coyote Lake and the 1971 San Fernando earthquakes. The parameters for the three

empirical source functions are summarized in Table 2. The displacement spectrum of each of these source functions was normalized to a Brune source spectral shape. A study of source scaling characteristics (Somerville *et al.*, 1987, this volume) showed that the source characteristics of eastern North American earthquakes are comparable with those in western North America. Their study did not include a comparison of the higher frequency source characteristics, so we have assumed that these are comparable.

The seismograms computed using the three different empirical source functions for both a 45° dip-slip mechanism and for a vertical strike-slip mechanism at a range of 250 km seen at 45° azimuth are shown in Figure 14. The differences in the corner frequencies of these source functions are illustrated by the different frequency content of the synthetic seismograms. The L_g magnitudes (at 250 km) for the 45° dip-slip mechanism obtained by averaging the values over 15° increments of azimuth from New Hampshire, Coyote Lake, and San Fernando empirical source functions are 5.18, 6.02, and 6.65, respectively. These values for the vertical strike-slip orientation are 4.81, 5.65, and 6.27, respectively. The azimuthally averaged magnitudes for both focal orientations are shown in Figure 12. The synthetic L_g magnitudes are in good agreement with the trend of the observations. It is expected that slightly different magnitude values might be obtained if empirical source functions from different recording stations, or from different events having the same seismic moments, were used in the generation of the synthetic seismograms.

Discussion

The identification of strong Moho reflections was also made in ground motion recordings of Western United States events. Figure 15 shows generalized ray

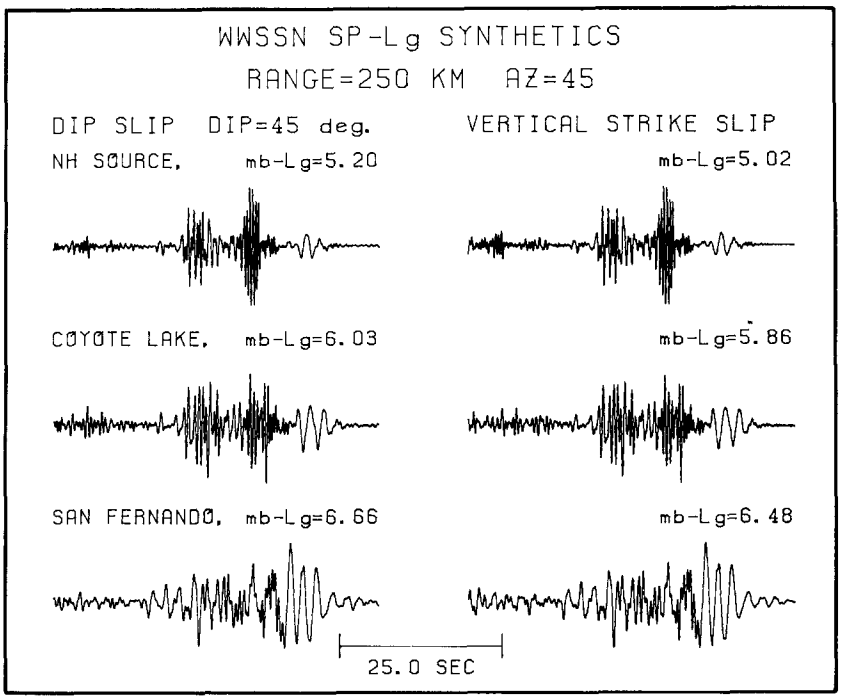

FIG. 14. Synthetic L_g waves and magnitudes for a 45° dip-slip fault and a vertical strike-slip fault using empirical source functions obtained from the New Hampshire, Coyote Lake, and San Fernando earthquakes. The synthetic seismograms are for a distance of 250 km seen at 45° azimuth.

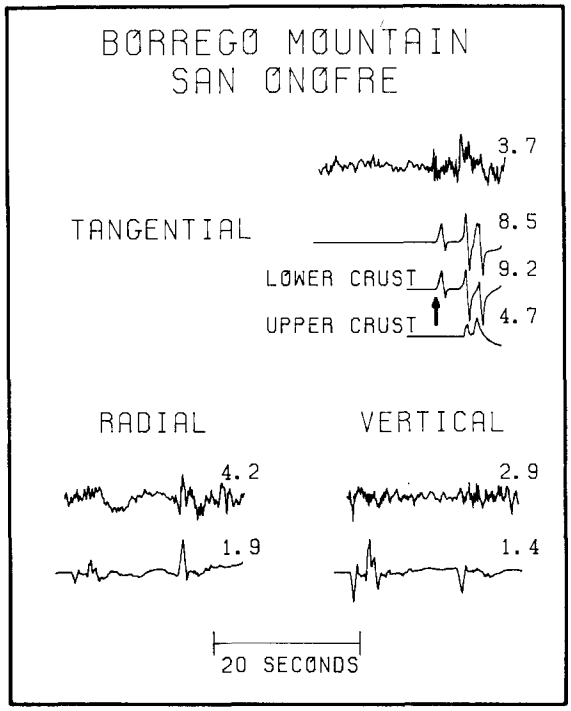

FIG. 15. Comparison of the velocity seismograms recorded at San Onofre (135 km) from the 1968 Borrego Mountain earthquake (*top*) with generalized ray synthetic seismograms (*bottom*). Shown below the tangential synthetic seismogram is a decomposition into rays that bottom in the lower crust (*upper trace*) and the rays confined to the upper crust (*lower trace*). Peak amplitudes are given in centimeters/second.

TABLE 4

BORREGO MOUNTAIN CRUSTAL MODEL

P Velocity (km/sec)	*S* Velocity (km/sec)	Density (gm/cm^3)	Thickness (km)	*Q*-alpha	*Q*-beta
2.5	1.6	1.4	0.4	500	250
5.1	3.0	2.3	2.5	1000	500
6.0	3.5	2.7	11.1	1000	500
7.1	4.2	3.2	11.0	1000	500
7.9	4.6	3.6	—	1000	500

synthetic velocity seismograms compared with observed velocity motions from the 1968 Borrego Mountain earthquake recorded at San Onofre (range = 135 km, azimuth = −70°). The crustal structure in the vicinity of Borrego Mountain (after Hamilton, 1970) is given in Table 4. The Q structure is assumed, but is not important considering the small range. The seismic moment (1.8×10^{26} dyne-cm), focal mechanism (strike = −45°, dip = 81°, and rake = 178°), source depth (8 km), and source-time history (triangle with 0.5 sec rise and 4.5 sec fall) are from Burdick and Mellman (1976). While the overall character of both the P and S waves is matched by this simple model, the frequency content is not as well matched. This is expected since the high-frequency components of the source were not included. Shown below the tangential synthetic seismogram is a ray decomposition of the waveform. The upper trace (lower crust) contains only those rays that bottom below the source

depth, including the reflections off the Moho (25 km) and the 14-km-deep interface. The lower trace (upper crust) contains only those rays that travel entirely above the source depth. Those rays that reflect off the 14 km and Moho discontinuities are shown to be the largest arrivals in the waveform. In particular, the first pulse (shown by the arrow) is the S wave that is postcritically reflected from the Moho. This feature is clear in the data and demonstrates that postcritical S waves reflected at the Moho are important in the strong ground motions of earthquakes in the Western United States as well as in the east.

The distance dependence of the local magnitude (M_L) scale often gives insight to strong ground motion attenuation (e.g., Trifunac, 1976; Kanamori, 1978). Bakun and Joyner (1984) developed an M_L scale for central California describing the log–amplitude decay with distance as the smoothly decreasing function $(-n\log R - kR)$, where n and k are constants determined for the region of interest and R is hypocentral distance. The first term represents the geometrical attenuation, and the second term represents anelastic attenuation. However, the magnitude residuals as a function of distance show large positive values (about 0.1 to 0.2 units) between 75 and 125 km in central California. These residuals may reflect the effect of earth structure on the M_L scale that was neglected in the analysis. Bakun and Joyner (1984) suggest that the bump in the M_L scale might be explained by the effects of crustal and upper mantle structure, in particular by reflections off the Moho. Our simulations support this conclusion. Dominant, large-amplitude reflections from the lower crust are apparent in refraction data from central California (Walter and Mooney, 1982), further suggesting that Moho reflections may be responsible for the bump in the M_L scale.

The results of the simulation of ground motions in eastern North America demonstrate that crustal structure can influence strong-motion attenuation relations. The region of high amplitudes observed between 60 and 150 km may be attributed to S waves postcritically reflected at the Moho. The range at which S waves become postcritical is dependent on the crustal thickness and velocity gradients. Our maritime Canada model predicts that the range of high amplitudes will occur between 100 to 200 km, while the Central United States crustal model predicts that the range will be about 60 to 150 km. The maritime Canada structure model contains a sharp discontinuity at 30 km depth and therefore produces a strong arrival due to reflections from this boundary. This velocity increase (as well as others) may extend over several kilometers. The effect of a velocity gradient rather than a discontinuity as used in this study would be to broaden the reflected pulse. The effect of more realistic crustal models, such as ones with velocity gradients, on attenuation relations should be investigated.

The effect of intrinsic attenuation (Q) on the attenuation relations should also be investigated. Campillo *et al.* (1984, 1985) have demonstrated that the effect of intrinsic attenuation on L_g is small for distances up to about 250 km, but becomes evident at greater ranges. Thus, the region of high amplitudes that may occur between about 60 and 200 km should be relatively unaffected by Q. Beyond this range, the effects of velocity structure may be obscured by those of intrinsic attenuation.

Several studies have investigated the effect of varying focal mechanism on L_g attenuation relations (e.g., Herrmann and Kijko, 1983a; Campillo *et al.*, 1984). For example, Campillo *et al.* (1984) found that vertical strike-slip and 45° thrust orientations produce identical L_g waveforms and, therefore, amplitude decay rates

with distance. However, the absolute amplitude of the L_g waves are larger for the dip-slip case. This result is confirmed by our results. The L_g waves for the 45° thrust and the vertical strike-slip mechanisms (Figure 14) have the same waveforms, but the dip-slip magnitudes are larger (see also Figure 12). Thus, the possible scatter in the amplitude data induced by focal mechanism variability may influence attenuation relations. This effect has been incorporated into the analysis given in Figure 11 and is shown to be substantial. Campillo *et al.* (1984) have shown that the form of the amplitude decay of L_g with distance is independent of source depth, but that the L_g excitation is weaker for events in the lower crust. Finally, the attenuation relations may also depend on the source corner frequency, particularly at larger distances where intrinsic attenuation becomes more important.

Conclusions

Synthetic strong-motion seismograms have been generated that are in good general agreement with strong-motion recordings in eastern North America and provide insight into the interpretation of these recordings. Moho reflections (i.e., postcritically reflected S waves from the crust-mantle transition) may have a significant influence on strong ground motion amplitudes at distances of approximately 100 km. The effect of this seismic phase is to arrest the decay of ground motion amplitude with distance over a specific range of distances. This is apparent in the observed data over the distance range of 60 to 150 km and occurs over the same distance range in the synthetic seismograms calculated using the Central United States crustal model. The corresponding distance range of 100 to 200 km in the synthetic seismograms calculated using the maritime Canada crustal model reflects the difference in the velocity contrast at the Moho in that model.

The implications of including the effects of postcritical Moho reflections in the construction of ground motion attenuation relations are illustrated by the curve in Figure 6. The initial decay of pseudo-velocity with distance from 10 to 60 km is not well constrained by the observed data, but is consistent with the synthetic attenuation relation. The interval of constant pseudo-velocity from 60 to 150 km may be due to strong Moho reflections. The range at which these reflections become postcritical is the key in determining the range of high amplitudes. After the reflection becomes postcritical, that arrival resumes a normal amplitude decay with distance, but the effect is to create a shoulder in the attenuation relation. This is seen in the observed data in Figure 6 and is illustrated by the synthetic attenuation relations in Figures 7, 10, and 11.

The L_g magnitudes measured from synthetic seismograms for a range of seismic moments are in good agreement with empirical data relating m_{bLg} and seismic moment. We have shown that, by using empirical source functions and considering wave propagation phenomena, we can generate synthetic seismograms having realistic L_g magnitudes and waveforms. Further improvement in agreement is expected if more adequate crustal structure models are used and scattering phenomena are included in the calculation of synthetic seismograms.

Acknowledgments

The authors thank C. B. Crouse and the anonymous reviewer for their comments. We are very grateful to R. Halliday and W. Shannon of the Earth Physics Branch of the Energy, Mines and Resources of Canada for providing seismograms. This study was sponsored by the Electric Power Research Institute.

REFERENCES

Bakun, W. H. and W. B. Joyner (1984). The M_L scale in central California, *Bull. Seism. Soc. Am.* **74,** 1827–1843.

Barker, J. S. (1984). A seismological analysis of the May, 1980, Mammoth Lakes earthquakes, *Ph.D. Thesis,* The Pennsylvania State University, University Park, Pennsylvania, 278 pp.

Boore, D. M. (1983). Stochastic simulation of high-frequency ground motions based on seismological models of their radiated spectra, *Bull. Seism. Soc. Am.* **73,** 1865–1894.

Bouchon, M. (1982). The complete synthesis of seismic crustal phases at regional distances, *J. Geophys. Res.* **87,** 1735–1741.

Brune, J. N. (1970). Tectonic stress and the spectra of seismic shear waves from earthquakes, *J. Geophys. Res.* **75,** 4997–5009.

Burdick, L. J. and G. R. Mellman (1976). Inversion of body waves of the Borrego Mountain earthquake to the source mechanism, *Bull. Seism. Soc. Am.* **66,** 1485–1499.

Campillo, M., M. Bouchon, and B. Massinon (1984). Theoretical study of the excitation, spectral characteristics, and geometrical attenuation of regional seismic phases, *Bull. Seism. Soc. Am.* **74,** 79–90.

Campillo, M., J.-L. Plantet, and M. Bouchon (1985). Frequency-dependent attenuation in the crust beneath central France from L_g waves: data analysis and numerical modeling, *Bull. Seism. Soc. Am.* **75,** 1395–1411.

Eckert, A. and G. Atkinson (1985). Ground motion data in eastern North America, in *Seismic Hazard Methodology for Nuclear Facilities in the Eastern United States,* Vol. 3, Appendix B, pp. B-1 through B-36, EPRI Research Project Number P101–29.

Electric Power Research Institute (1985). *Earthquake Catalog for the Eastern United States,* Seismicity Owners' Group, Seismic Hazards Research Program.

Hadley, D. M., D. V. Helmberger, and J. A. Orcutt (1982). Peak acceleration scaling studies, *Bull. Seism. Soc. Am.* **72,** 959–979.

Hamilton, R. M. (1970). Time-term analysis of explosion data from the vicinity of the Borrego Mountain, California, earthquake of 9 April 1968, *Bull. Seism. Soc. Am.* **60,** 367–381.

Hanks, T. C. and R. McGuire (1981). The character of high-frequency strong ground motion, *Bull. Seism. Soc. Am.* **71,** 2071–2095.

Helmberger, D. V. and S. D. Malone (1975). Modeling local earthquakes as shear dislocations in a layered half space, *J. Geophys. Res.* **80,** 4881–4888.

Helmberger, D. V. and D. G. Harkrider (1978). Modeling earthquakes with ray theory, in *Modern Problems in Elastic Wave Propagation,* J. Miklowitz and J. D. Achenbach, Editors, John Wiley and Sons, New York, 499–518.

Herrmann, R. B. (1985). An extension of random vibration theory estimates of strong ground motion to large distances, *Bull. Seism. Soc. Am.* **75,** 1447–1453.

Herrmann, R. B. and A. Kijko (1983a). Modeling some empirical vertical component L_g relations, *Bull. Seism. Soc. Am.* **73,** 157–171.

Herrmann, R. B. and A. Kijko (1983b). Short-period L_g magnitudes: instrument, attenuation, and source effects, *Bull. Seism. Soc. Am.* **73,** 1835–1850.

Kanamori, H. (1978). Semi-empirical approach to prediction of ground motions produced by large earthquakes, *Proc. NSF Seminar Workshop on Strong Ground Motion,* California Institute of Technology, Pasadena, California, 80–84.

Langston, C. A. (1978). The February 9, 1971 San Fernando earthquake: a study of source finiteness in teleseismic body waves, *Bull. Seism. Soc. Am.* **68,** 1–29.

Langston, C. A. (1982). Aspects of *Pn* and *Pg* propagation at regional distances, *Bull. Seism. Soc. Am.* **72,** 457–471.

Liu, H.-L. and D. V. Helmberger (1983). The near-source ground motion of the 6 August 1979 Coyote Lake, California, earthquake, *Bull. Seism. Soc. Am.* **73,** 201–218.

Sauber, J. M. (1984). The January 19, 1982, Gaza, New Hampshire earthquake, in *A Study of New England Seismicity with Emphasis on Massachusetts and New Hampshire,* Technical Report covering 1982–1984, Earth Resources Laboratory, Massachusetts Institute of Technology, Cambridge, Massachusetts, 104 pp.

Somerville, P. G., J. P. McLaren, L. V. Lefevre, R. W. Burger, and D. V. Helmberger (1987). Comparison of source scaling relations of eastern and western North American earthquakes, *Bull. Seism. Soc. Am.* **77,** 322–346.

Trifunac, M. D. (1976). Preliminary analysis of the peaks of strong earthquake ground motion—

Dependence of peaks on earthquake magnitude, epicentral distance, and recording site conditions, *Bull. Seism. Soc. Am.* **66,** 189–219.

Walter, A. W. and W. D. Mooney (1982). Crustal structure of the Diablo and Gabilan ranges, central California: a reinterpretation of existing data, *Bull. Seism. Soc. Am.* **72,** 1567–1590.

WOODWARD-CLYDE CONSULTANTS
566 EL DORADO STREET
PASADENA, CALIFORNIA 91101
(R.W.B., P.G.S., J.S.B.)

DEPARTMENT OF EARTH AND
ATMOSPHERIC SCIENCES
SAINT LOUIS UNIVERSITY
P.O. BOX 8099, LACLEDE STATION
SAINT LOUIS, MISSOURI 63156 (R.B.H.)

SEISMOLOGICAL LABORATORY
CALIFORNIA INSTITUTE OF TECHNOLOGY
PASADENA, CALIFORNIA 91125 (D.V.H.)

Manuscript received 19 February 1986